SAND2014-19047R

SAND - 2014-XXXX P

Unknown
Field Code Changed

Unknown
Field Code Changed

Unknown
Field Code Changed

Progress report of Sandia National Laboratories (SNL) contribution to IAEA CRP F11016 on "Utilization of ion accelerators for studying and modeling of radiation induced defects in semiconductors and insulators", 3rd RCM

György Vízkelethy
Sandia National Laboratories
Department of Ion-Solid Interactions
Albuquerque, NM 87185-1058, USA

Sandia National Laboratories is a multi-program laboratory managed and operated by Sandia Corporation, a wholly owned subsidiary of Lockheed Martin Corporation, for the U.S. Department of Energy's National Nuclear Security Administration under contract DE-AC04-94AL85000.

Sandia National Laboratories

U.S. DEPARTMENT OF ENERGY

Vizkelethy, Reviewer 10/22/2014 3:46 PM
Deleted: 3

Vizkelethy, Reviewer 10/22/2014 3:46 PM
Deleted: 4

Vizkelethy, Reviewer 10/22/2014 3:46 PM
Deleted: 4

Vizkelethy, Reviewer 10/22/2014 3:46 PM
Deleted: 7

Vizkelethy, Reviewer 10/22/2014 3:46 PM
Deleted: 8

Vizkelethy, Reviewer 10/22/2014 3:46 PM
Deleted: 10

Vizkelethy, Reviewer 10/22/2014 3:46 PM
Deleted: 13

Vizkelethy, Reviewer 10/22/2014 3:46 PM
Deleted: 16

Vizkelethy, Reviewer 10/22/2014 3:46 PM
Deleted: 16

Vizkelethy, Reviewer 10/22/2014 3:46 PM
Deleted: 17

Vizkelethy, Reviewer 10/22/2014 3:46 PM
Deleted: 20

Vizkelethy, Reviewer 10/22/2014 3:46 PM
Deleted: 22

Introduction

This report presents the results of Sandia National Laboratories' (SNL) contribution to IAEA CRP F11016 as mostly raw data. The goal of this CRP is to study the effects of radiation on semiconductors and insulators with the emphasis on the effect of displacement damage due to MeV energy ions on the performance of semiconductor detectors and microelectronic devices. SNL is tasked with performing electrical characterization, irradiation, and IBIC, DLTS, C-V measurements on devices used in the CRP, as well as calculating damage and ionization profiles for modeling. In this period the following work was accomplished:

- Evaluation of whole area irradiation of Helsinki diodes and S5821 Hamamatsu PIN diodes using C-V, Deep Level Transient Spectroscopy (DLTS), and Ion Beam Induced Charge (IBIC) measurement. The irradiations were performed at ANSTO [1].
- Neutron irradiation of Helsinki diodes at the SNL Annual Core Research Reactor (ACCR) and analysis of the diodes using C-V and IBIC measurements. The main goal was to evaluate the effect of whole area irradiation.
- In the previous reports it was indicated that the model created by the CRP was failing. Also, from the previous whole area irradiations it became evident that even small fluences can cause significant increase in leakage current. This leakage current can prevent the diode getting biased due to the large protection resistor in the preamplifier used for IBIC measurement. We investigated several Hamamatsu diodes to determine whether they would be better subjects of the CRP. They were irradiated with neutrons at ACRR and characterized by C-V and IBIC.
- The damage model in Marlowe was reinvestigated. It was found that the EBND parameter was incorrectly used as the displacement energy while it is really the bulk binding energy. A new method was developed to determine a recombination radius to more precisely determine the displacement damage. Although this work was mainly done for another project, this CRP also benefits from it.
- To compare the CRP's model we decided to do TCAD calculations to model IBIC in the Helsinki diodes. At first a 2D model of a small piece of the diode was created, and we found a large plasma effect. The electric field was pushed out from the e-h plasma and charge induction process lasted up to a few μs. As the next step, we created a model for the full size diode based on the model created at University of New Delhi [2]. IBIC simulations of 2 MeV He ions were performed for both the small and full diode structures to study how the size of the device changes the plasma effect.

IBIC and C-V characterization of 8 MeV He whole area irradiated Helsinki and Hamamatsu diodes

C-V and DLTS measurements

An n-type Helsinki diode and two Hamamatsu S5821 PIN diodes were irradiated with 8 MeV He ions at ANSTO. The He ion beam was rastered over the devices with ~ 10,000 ions/s, 500 µs dwell time and ~2 µm pixel size. The irradiation patterns are shown in Figure 1.

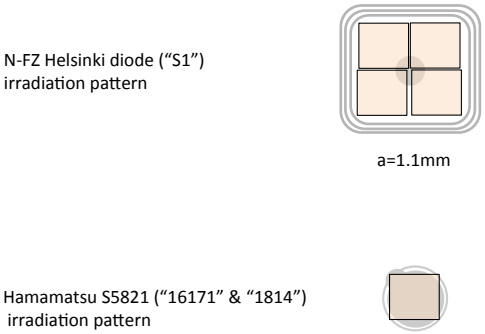

Figure 1 Irradiation patterns for the Helsinki and S5821 PIN diodes

The area of the devices and the irradiation fluence is shown in Table 1, for further details see [1].

Table 1 Irradiation fluences and areas

Device	Area [mm²]	Fluence
N_FZ Helsinki	2.5x2.5	1E+10
S5821 #16171	1.1	1E+10
S5821 #1814	1.1	1E+09

The exact properties of the S5821 diodes are not known apart from the parameters given in the spec sheet available at the Hamamatsu website. Using the parameters and the C-V curve from the spec sheet, we determined that the doping in the intrinsic layer is in order of 10^{13} 1/cm^3 and the depletion layer is around 45 µm at 50 V. At first C-V measurements were performed on all three devices.

Figure 2 shows the C-V curves before and after irradiation. The pre irradiation curve for the Helsinki diode is from another similar diode, and for the S5821 PINs the C-V curve from the spec sheet was used. The change in the capacitance of the Helsinki diode is somewhat larger than the change in a diode irradiated with the 8 MeV He ions at SNL using the pulsed irradiation facility (25 pF ANSTO vs 40 pF SNL) [3]. The reason for the discrepancy can be attributed to the fact that the pulsed irradiation

might not enterily cover the device; therefore, the real fluence was probably somewhat lower than the nominal one.

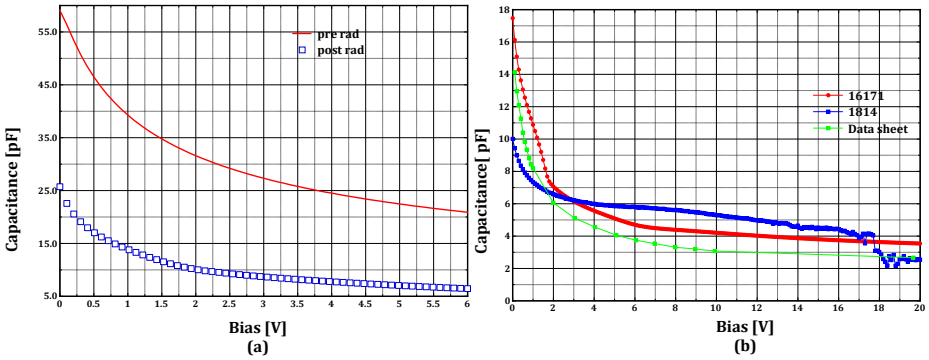

Figure 2 C-V curves before and after irradiation, Helsinki diode (a), S5821 PINs (b)

The C-V curves for the S5821 PINs are more confusing. The un-irradiated C-V curves measured at ANSTO agree quite well with the one from the spec sheet. The usual behavior of the capacitance at 0 V is a decrease in capacitance after the irradiation. For moderate damage usually the capacitance approaches the un-irradiated one at increasing voltages, and for higher damages it was observed that the capacitance after irradiation becomes larger than the un-irradiated one for higher bias values. In this case the behavior of the C-V curves is inconsistent. The lower fluence irradiation (#1814 @ 10^9 ions/cm^2) mimics a high damage case. The higher fluence irradiation (#16171 @ 10^{10} ions/cm^2) does not make much sense; the capacitance increased at 0 V bias. It might be necessary to repeat this experiment.

DLTS measurements were performed on all three devices. The measurement was quite problematic with the Helsinki diode because of its size. The SNL DLTS equipment is designed for devices mounted in TO-18 cans.

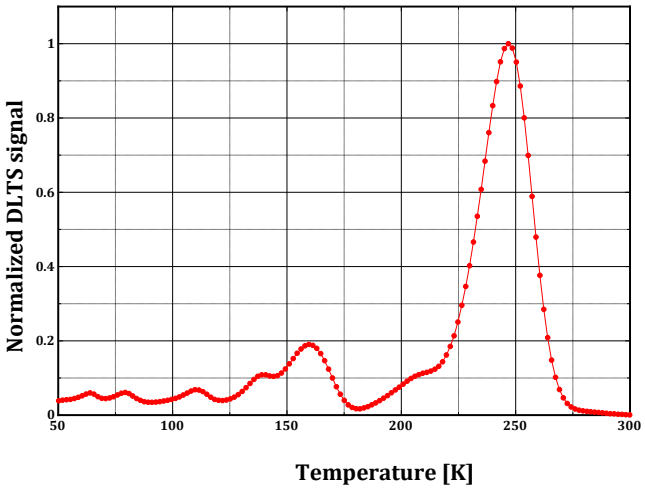

Figure 3 DLTS Spectrum of Helsinki diode after 8 MeV He irradiation

Figure 3 shows a DLTS spectrum of the Helsinki diode. The absolute temperature scale is incorrect, since the device did not have very good heat contact. The spectrum is a usual Si displacement damaged spectrum with the asymmetric V2(--) and V2(-) peaks (see for example [4]). One noticeable feature of the spectrum is the lack of the VO peak at low temperatures, which can be attributed to defect compensation.

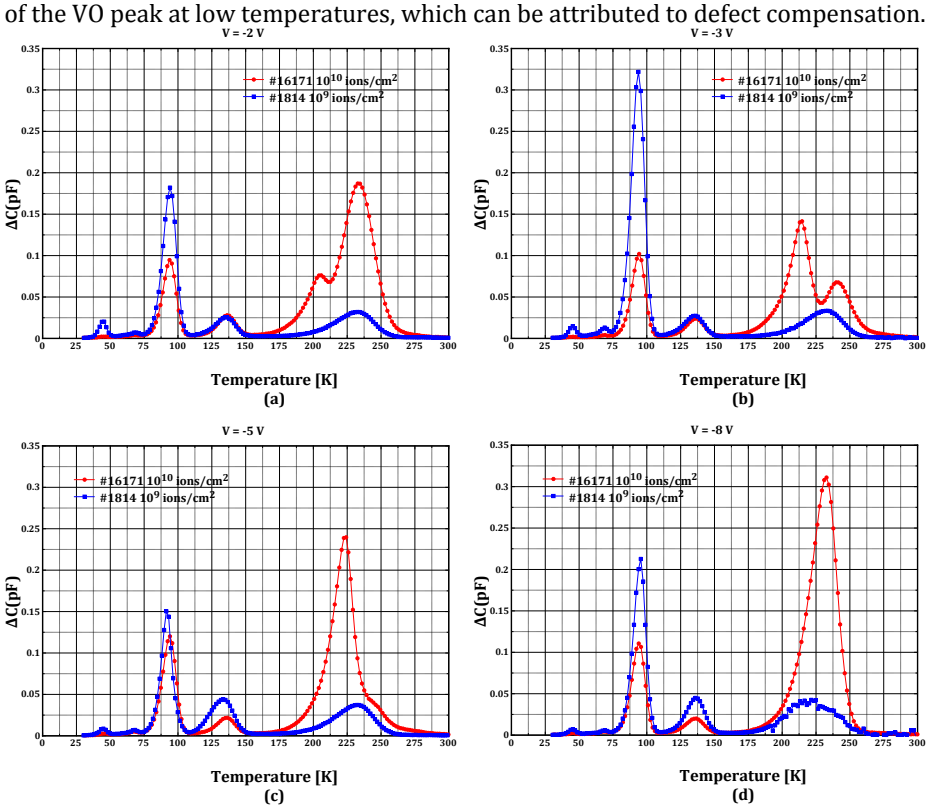

Figure 4 DLTS spectra of S5821 #1814 and #16171 at various bias voltages

Figure 4 shows DLTS spectra of the two S5821 PINs at various bias voltages. By increasing the bias, DLTS probes thicker and thicker layers. With the -2 V to -8 V range the region probed varied from 15 to 20-25 μm. Let's recall that a 8 MeV He ion created the end of range damage (peak in the damage profile) at around 50 μm and it is about 5 μm wide [3]. Therefore it is obvious that DLTS is probing only the region where the damage is uniform and relatively low. What we expect is that the DLTS peaks are growing with increasing bias voltage (more defects are included in the sensitive region). We definitely do not expect a change in the shape of the spectrum. The spectra of #1814 follow quite well this expected behavior. The spectrum shows two V2 peaks with about the same height (indicates no clustering), and they are slowly growing with increasing bias. On the other hand the spectra of #16171 show peaks moving around, which are not the well known DLTS peaks. The C-V curve of #16171 already indicated that there is some problem with this device, and the DLTS

measurement confirmed it. Unfortunately, we do not know much about the structure of the device (such as oxides or passivation layers). One possibility (apart from experimental error) is that there is an oxide layer that has trapped charge in it. This beam generates large amount of electron-hole pairs, of which the holes can be trapped in the oxide and affect both the C-V and DLTS measurements.
At this point it is interesting to have another look at Figure 3. It is quite different from the spectrum of #1814. The DLTS spectrum of #1814 is electron like, while the spectrum of the Helsinki diode is more like the spectrum of a neutron or heavy ion irradiated device. The Helsinki diodes are very low doped (almost two orders of magnitude lower than the S5821) and they are practically depleted to 50 µm at 0V. Applying any voltage will increase the depletion layer further. Since the damage peak is right around 50 µm, the DLTS is actually measuring the end of range damage peak and not the uniform low damage region. The spectrum's shape indicates that at the end of range the damage is more neutron like.
The C-V and DLTS data were sent to RBI and ANSTO for further processing and interpretation.

IBIC measurements

The Helsinki diode got damaged during DLTS measurement; therefore, no IBIC measurement was performed on it. We performed IBIC measurements at 2, 5, and 10 MeV energies. We compared the induced charge to the charge induced in a Hamamatsu S1223 PIN diode, which we routinely use for calibration.

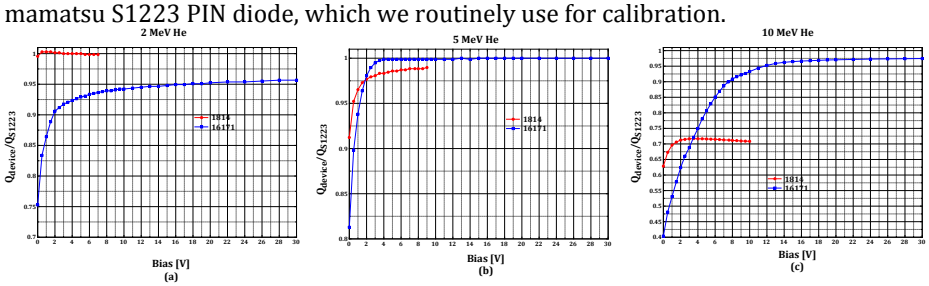

Figure 5 CCE bias curves for 2 MeV (a), 5 MeV (b), and 10 MeV (c) He ions

Figure 5 shows the CCE bias curves for the three energies. Unfortunately, due to the high leakage current of #1814 (although it had the lower fluence), the bias could not be increased over 10 V on this device. The qualitative interpretation of the bias curves for #1814 is relative simple. In the 2 MeV case all the charge is deposited in the depletion layer (which is already around 8 µm even at 0 V) and the induced charge is entirely due to drift. The damage is low enough not to have recombination; therefore, the CCE is very close to 1 and independent of the bias. In the case of 5 MeV the charge is deposited up to 20 µm. When the depletion region is larger than this distance, we have the same case as before, with full charge collection for moderate damage. Unfortunately, device #1814 could not be biased to reach this width due to the leakage current and the 100 MΩ protection resistor in the Ortec 142A preamplifier. When the depletion layer width is less, then only part of the charge is collected by drift, a fraction outside of the depletion layer has to diffuse into the de-

pletion layer, and during diffusion more recombination occurs due to the damage. As the depletion region width increases with bias, so does the CCE. In case of 10 MeV most of the charge is created behind the damage peak, so the carriers have to diffuse through the highly damaged region to reach the junction. Many of the carriers will recombine in the highly damaged region on their way to the depletion region. This explains the greatly reduced CCE.

The interpretation of the #16171 bias curves is more problematic. In principle, for the 2 MeV case the bias curves should have the same shape, although, lower CCE for #16171 if the damage close to the surface affects the recombination during drift. The different bias dependence suggests that the depletion depth dependence on the bias voltage is not the same for the two devices. Our suspicion is that trapped charge in the oxide causes the actual voltage on the device to be different than the applied one (this is not the same problem as above with the leakage current). More analysis of the data is required.

Finally, Figure 6 summarizes the collected charge for the two devices at the different energies at 0 V (built-in depletion layer) and at the saturation voltage. The 1223 PIN collected charge is included for reference. A simple conclusion is that at energies when the charge is generated between the surface and the high damage layer at high voltages the low damage (#1814) does not affect the charge collection. When most of the charge is created behind the high damage region, the charge collection decreases significantly even at high voltage.

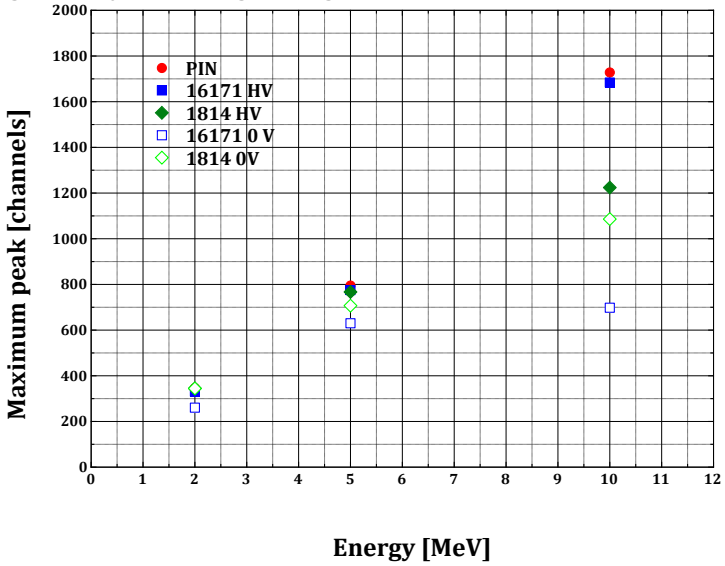

Figure 6 Maximum peaks channels at 0 V and at saturation

Characterization of neutron irradiated Helsinki diodes

Four p-type Helsinki diodes were irradiated with neutrons at the SNL ACCR up to $0.9x10^{14}$ 1 MeV neutron equivalent fluence.

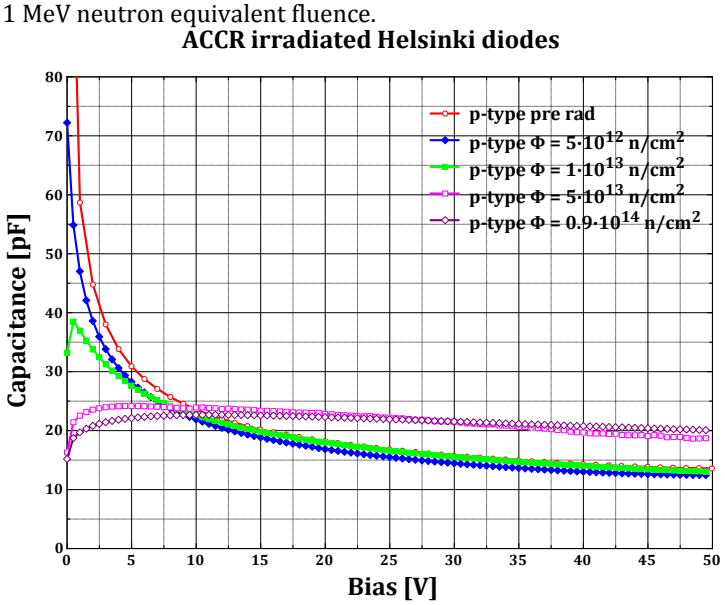

Figure 7 C-V curves of neutron irradiated p-type diodes

Figure 7 shows the C-V curves before and after the neutrons irradiation. It is clear that for the first two fluences the damage is moderate, the C-V curves change as expected, lower capacitance at zero bias and the capacitance gradually approaches the un-irradiated values at higher biases. On the other hand the higher fluences ($\geq 10^{13}$ n/cm^2) seemed to completely destroy the devices, and the C-V curve does not resemble a diode C-V curve anymore. It is somewhat surprising since Si bipolar junction transistors (BJTs) were operable at these fluences [5-7]. The higher sensitivity in this case can be probably attributed to the very low doping of the intrinsic layer.
We attempted to perform IBIC measurements on these diodes using a 2 MeV He beam. All diodes had large leakage current; therefore, we could not put more then a few volts on the device even with an applied bias of 100 V. For the two highest fluences the IBIC signal was in the noise, and nothing could have been measured. For the two lower fluences we could measure a CCE bias curve but we could not determine the actual voltage on the diodes due to the large leakage currents and not precise enough current measurements. Since the un-irradiated diodes are depleted to 50 µm at zero volt, the slowly increasing CCE indicates that the electrostatics of the diode has changed, probably due to charge trapped in the defects.

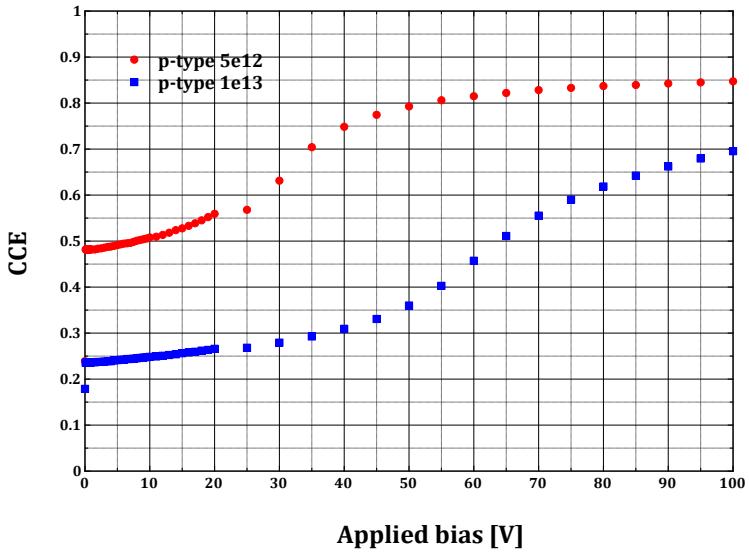

Figure 8 CCE vs. applied bias curves

Search for better devices

As we saw above and will see later, the Helsinki diodes are not ideal. Due the large size the leakage current becomes so large that it is impossible to bias them through the 100 MΩ protection resistor of the Ortec 142A preamplifier. Also, due to the very low doping, even at low damage the defect density can approach the doping density and the charge trapped it the defects can change the electrostatics of the device. Since the C-V and DLTS information is important in addition to the IBIC measurements, to avoid these problems we need to do separate full area irradiations for C-V and DLTS and microbeam irradiations for IBIC (although in this case the electrostatics still changes locally, but it is not clear how much problem this poses for modeling). In addition, due to the large size of these diodes the full area ion irradiation is difficult and time consuming. They have the one major advantage that we know quite a bit about the structure and the manufacturing process [8].

We considered three devices, two Hamamatsu PIN diodes (S5821 and S5973) and a Hamamtsu PN diode (S2368). We selected S5973 and S2386 because we already had them and structural analysis and doping profile determination were performed on them. The S5821 was selected because it was already used in the ANSTO full area irradiations. The devices were irradiated in the SNL ACCR with the same fluences as the p-type Helsinki diodes. This test seems to be the most brutal, since the damage is done in the entire volume of the diodes.

All three diodes are relatively small, with an area in order of 1 mm^2. The doping profile of S5793 and S2386 were measured in the past by spreading resistance measurements, and they are shown in Figure 9 with the bias dependence of the depletion depth.

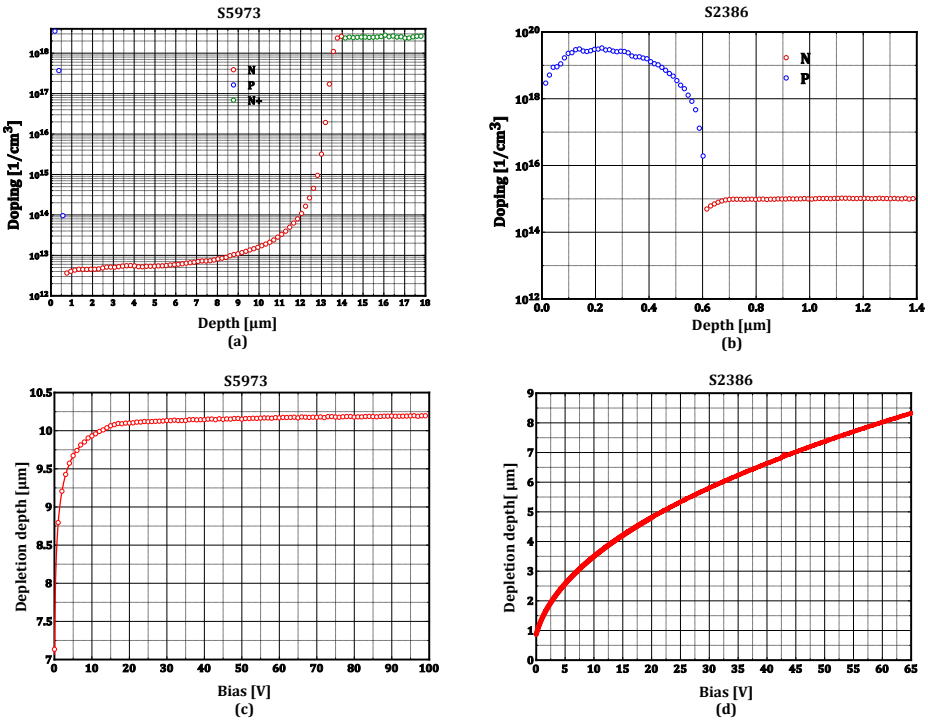

Figure 9 Doping profiles and depletion depth vs. bias for S5973 and s2386

The S5963 is PIN diode with a doping level of 0.5-1x10^{13} 1/cm^3 in an approximately 10 µm thick intrinsic layer. It is fully depleted at ~ 20 V and already 7 µm is depleted at 0 V (which means that at even 0 V all the charge from the 2 MeV He is created in the depletion layer. The S2386 is a P+N diode, which is depleted to 1 µm at 0 V and about 8.5 µm at 65 V. Above this bias the device started to break down. So in this device we were expecting to see a strong bias dependence of the CCE for 2 MeV He ions.

For the S5821 PIN we do not have a doping profile analysis, but the C-V curves indicate an intrinsic layer with a doping of ~10^{13} 1/cm^3. It also shows that the device is depleted to ~6 µm at 0 V and about 45 µm at 50 V.

We performed IBIC measurements with a 2 MeV He beam before the neutron irradiation as the function of bias voltage shown in Figure 10. The results are more or less what was expected; for the PIN diodes there is practically no bias dependence, the depletion layer at 0 V is already thicker than the region where the He ion deposits the charge.

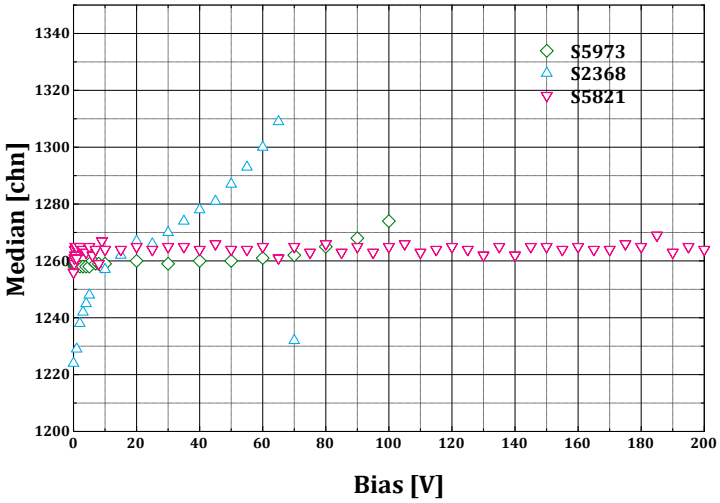

Figure 10 CCE bias curves for S5973, S5821, and S2386 before neutron irradiation

The S2386 also shows the expected bias dependence but after saturating it starts growing again and the IBIC signals becomes larger than the maximum available charge. This behavior indicates avalanches due to impact ionization.

The devices were irradiated with neutrons up to a 1 MeV neutron equivalent fluence of 0.9×10^{14}. During the irradiations three of the S5973 diodes became damaged. C-V measurements were performed on the remaining parts. The C-V curves for S2386 practically did not change at all; the C-V curves for the other devices are shown in Figure 11.

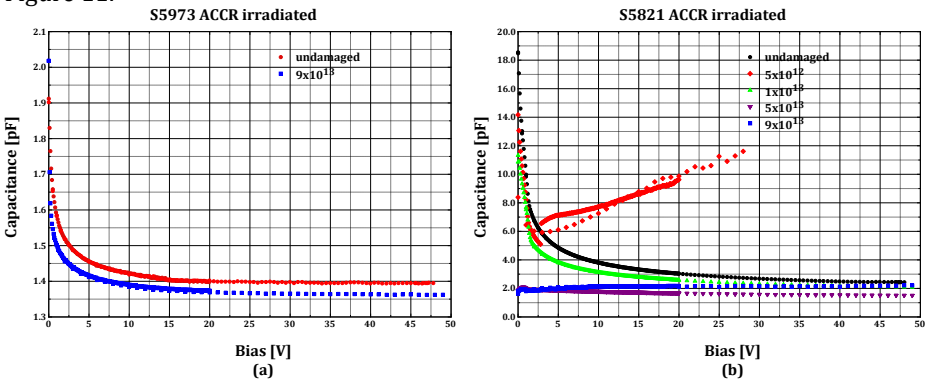

Figure 11 C-V curves for neutron irradiated S5973 and S5821 PINs

The C-V curve for the S5973 irradiated with the highest fluence showed very little change, but when it was placed in the vacuum chamber it became a short circuit. The C-V curves of S5821 indicates that something is wrong with the device irradiated with the lowest fluence, and the two highest fluences show that the devices are

practically dead. We performed IBIC on the three remaining S5821 PINs and all the four S2386 PNs, the bias curves are shown in Figure 12.

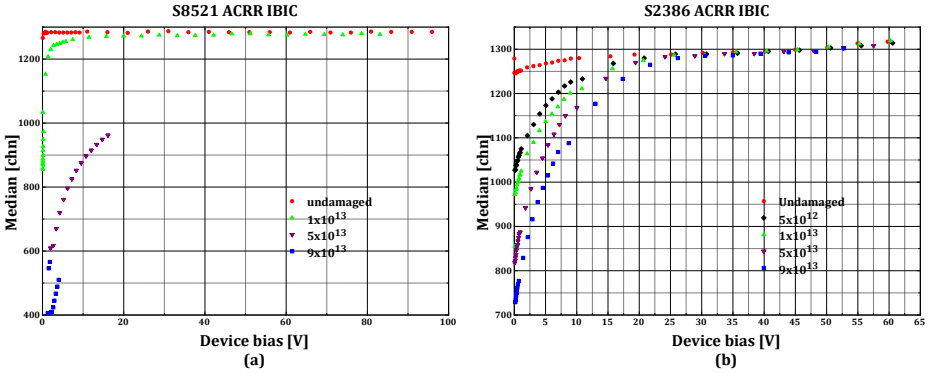

Figure 12 IBIC bias curves for neutron irradiated S8521 (a) and S2386 (b) devices

Although the high fluence S5821 devices seemed to be dead from the C-V curves, we could measure 70 % and 38 % charge collection efficiency at the highest bias we were able to put on. These devices had very large leakage current, several hundreds of nAs at less than 20 V. Also the shapes of the curves indicate that the damage (trapped charge) significantly changed the electrostatics of the device. The S2386 bias curves look exactly as expected. It is worth noting that the increase above the maximum deposited charge is still present, although it is harder to see due to the different scale. Based on the above we think that the S2386 would be a much better device for this project than any of the others, including the Helsinki diodes.

Improvement of damage calculations with Marlowe[1]

Most Binary Collision Approximation (BCA) codes use the concept of displacement energy, which is the energy that an atom has to overcome to be replaced permanently. Originally Marlowe used the same concept [9]. Unfortunately, most people read only this paper and use Marlowe based on it. In the 80s the code was changed and the displacement energy concept was removed and a pair classification scheme was introduced. The authors realized that the displacement energy is not a very good concept, at least not in this environment, and there is a better way to handle it. For example, in Si the displacement energy is dependent on the direction of the recoil, and it can be anything between 12 to 32 eV. Let me quote here Marc Hou (one of the contributors and frequent user of Marlowe) [10]:

"In the case of Frenkel pairs production, an energy threshold was found experimentally below which no Frenkel pair is produced. This suggests an energy threshold value for BCA computations. Unfortunately, this threshold value was found to be dependent on the direction in which momentum is given, which was also predicted by

[1] This work was mainly done for another project, but it has important implications for this CRP; therefore, we include here a brief description.

MD. Thus, depending on direction, the mechanisms involved in producing Frenkel pairs is different, and, therefore, its quantitative estimate for BCA calculations is ambiguous."

When an atom is displaced from its lattice site and stops in a non-lattice position it distorts the lattice. If there is a vacancy nearby, recombination puts the lattice in an energetically more preferable state, like the lattice "pushes" the interstitial into the vacancy [11]. The question is what is nearby? This nearby is what we can call the recombination radius discussed in several papers [12-16]. Marlowe's approach is to pair each interstitial with a vacancy and classify them as close, near, and distant pairs [17]. It assumes that anything other than the distant pairs will recombine in a very short (ps) time scale. This does not really define a recombination radius. Marlowe has three binding energies, specified in the EBND parameter.

- EBND(1) – this is the normal binding energy
- EBND(2) – this is the binding energy for an interstitial or impurity atom. It is not really important since the probability of a recoil colliding with another, stopped recoil is very, very low.
- EBND(3) – this is the binding energy in a replacement collision.

The argument using a different binding energy is that in a replacement collision the state of the lattice does not change; therefore, no energy needed to be removed from the energy of the moving atom. Initially 0 eV was used, but they found that it overestimates the displacements (compared to MD). Now it is said that it is a small amount, less than EBND(1). According to Robinson [18] EBND(1), the normal binding energy is the cohesion energy, which is 4.63 eV for Si

The first task was to determine what EBND(3) is. We calculated the total number of displacements with Molecular Dynamics (MD) and Marlowe, Si into Si at energies from 500 eV to 10 keV. In the Marlowe calculations we varied the EBND(3) parameters from zero to EBND(1). Then we picked the EBND(3) value that gave the closest number of total displacements to the MD calculations. The calculations gave 1.68 eV as the best EBND(3) value with a standard deviation of 0.13 eV.

The next step was to calculate the permanent Frenkel-pairs with MD. A Frenkel-pair was considered permanent if it was present at the end of the calculation (100 ps after the recoil was started). Marlowe calculations were performed and the separation distribution was created for all the pairs. Figure 13 shows the integrated separation distribution for the 5 energies we used in the calculations. What seemed surprising at first sight is that all five distributions are very similar, practically the same. Thinking about the recoil creation process a bit more gives the obvious explanation, which is that most of the vacancies are created by the low energy recoils whose distribution is independent of the initial particle energy (at least in this energy range). We compared the number of permanent Frenkel-pairs from the MD calculation to these distributions and determined a cut-off distance. This distance turned out to be 7.4±0.09 Å, 1.36 times the Si lattice constant.

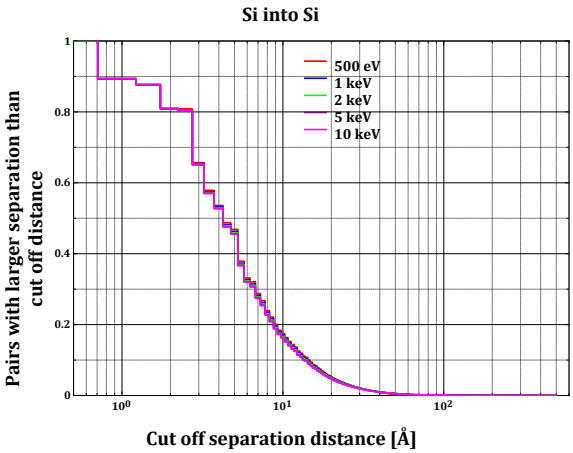

Energy	Cut-off distance
500	7.44
1000	7.42
2000	7.25
5000	7.41
10000	7.47
Average	7.398
Stdev	0.086
Percentage	1.16%

Figure 13 Separation distance distribution

It is interesting to see how the number of permanent Frenkel-pairs distributed between the different Marlowe pair classes. Table 2 shows what fraction of the different classes of Marlowe pairs survived the cut-off process. Not surprisingly the near and close pairs were all eliminated by that process. However, almost all correlated distant pairs were also eliminated (> 95 %). On the average, only ~50 % of the distant pairs become permanent Frenkel-pairs, so Marlowe overestimates the damage by a factor of two if one considers all the distant pairs. More details can be found in [19].

Table 2 Survival rate of different classes of Marlowe pairs[2]

	500 eV						
	Correlated close	Uncorrelated close	Correlated near	Uncorrelated near	Correlated distant	Uncorrelated distant	Total
Recombined	3.97	1.31	3.97	6.19	4.17	6.22	25.83
Survived	0.00	0.00	0.00	0.00	0.22	9.88	10.10
Survival ratio	0.00%	0.00%	0.00%	0.00%	4.99%	61.39%	28.11%
	10 keV						
	Correlated close	Uncorrelated close	Correlated near	Uncorrelated near	Correlated distant	Uncorrelated distant	Total
Recombined	65.84	25.19	65.84	115.90	64.96	109.64	447.38
Survived	0.00	0.00	0.00	0.00	2.96	157.38	160.35
Survival ratio	0.00%	0.00%	0.00%	0.00%	4.36%	58.94%	26.38%

[2] Correlated pairs have the interstitial originated from the paired vacancy, uncorrelated do not.

TCAD (ATLAS) modeling of the Helsinki diodes

In order to check the CRP's 1D model of IBIC in damaged Si diodes we used ATLAS [20] to model the diode in 2D. We created a full-length diode but only 20 μm wide to minimize the number of nodes needed. The initial IBIC calculations showed a huge plasma effect, the e-h plasma pushed out the electric field outside of the plasma and the IBIC current lasted up to a few μs. The electric field was restored when the plasma density became comparable to the doping density. This was very troubling because the electric field changed drastically and the CRP model assumes that the e-h plasma does not disturb the field. Since the decrease in the e-h plasma density was due to its diffusion, the size of the simulated device can have a large effect.

Electrostatic model of the device

After consulting with S. Rath (University of New Delphi was also working on an ATLAS simulation, although not IBIC) we decided to adopt their model [2]. They were modeling half of the entire device with all the guard rings. We decided to model the entire device width to investigate the plasma effect. Unfortunately, ATLAS did not let us do that; it has a node limit and the guard ring implantations used up too many nodes. Since none of the experiments were using the guard ring we eliminated them. We studied the effect of the guard ring and the size of the device on the electrical parameters of the diode and found that there is very little effect. The doping profiles were taken from [21] with changing the doping density in the intrinsic layer to 3.07×10^{11} 1/cm^3. This value gave the best agreement with the measured C-V data. In the University of New Delhi simulation the leakage current was orders of magnitude lower than the measured one. We found that was due to the very long carrier lifetime they used. We varied the carrier lifetime and found that 380 μs gives a very good agreement with the experimental data. We have to note that this value is an order of magnitude smaller than the one given in [8].

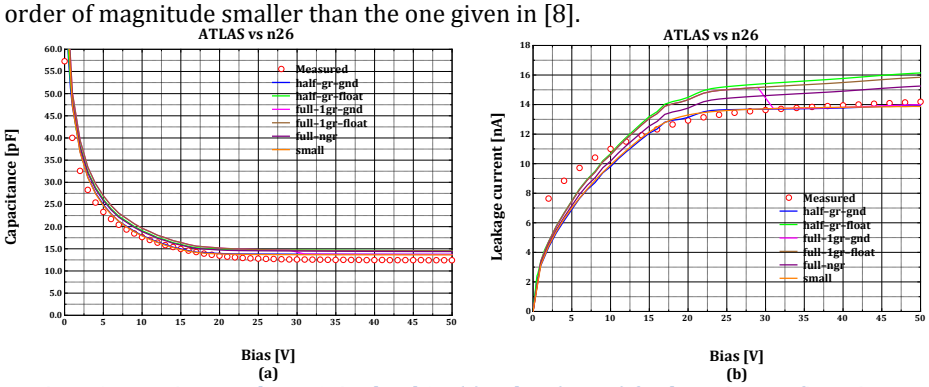

Figure 14 Experiment and ATLAS simulated C-V (a) and I-V (curves) for the various configurations

Figure 14 shows the ATLAS calculated C-V and I-V curves in the different configurations[3] compared to the measured data on diode #28 (n-type). The model shows excellent agreement with the experimental data and practically there is no difference between the different configurations. The calculated electric field, potential, and carrier densities are in good agreement with E. Vittone's 1D model [21].

IBIC simulation

We modeled the IBIC signal due to a 2 MeV He ion strike at 50 V bias. The device is completely depleted at this bias. ATLAS needs an electron-hole generation term as the functions of space and time (it is a C function that the ATLAS C interpreter compiles for the software). We calculated the 2D ionization energy loss profile using SRIM [22] (it has more precise stopping power than Marlowe) and fitted to a Gaussian around the center of the track with the standard deviation as the function of depth. Figure 15 shows the depth dependence of the charge created per unit length and the spread around the center of the track. This is the spatial dependence of the generation term. SRIM cannot provide temporal information, but fortunately Marlowe can. Figure 16 shows the probability distribution of the slow down time for 200,000 He ions. The median of the distribution is ~ 3 ps, which we chose as the duration of the e-h generation.

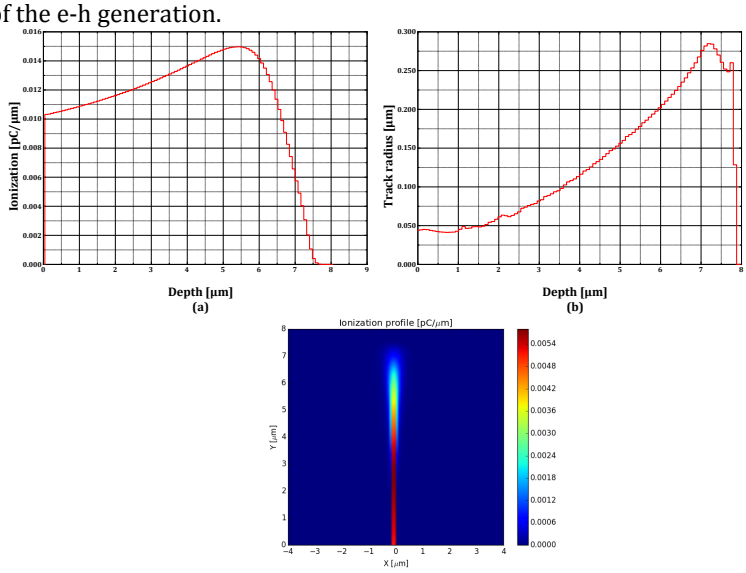

Figure 15 Depth dependence of ionization loss and radial spread

[3] The different configurations were: half diode with 1 guard ring grounded and floating scaled up to the full diode, full diode with 1 guard ring grounded and floating, full diode no guard ring, 20 μm diode scaled up to the full diode.

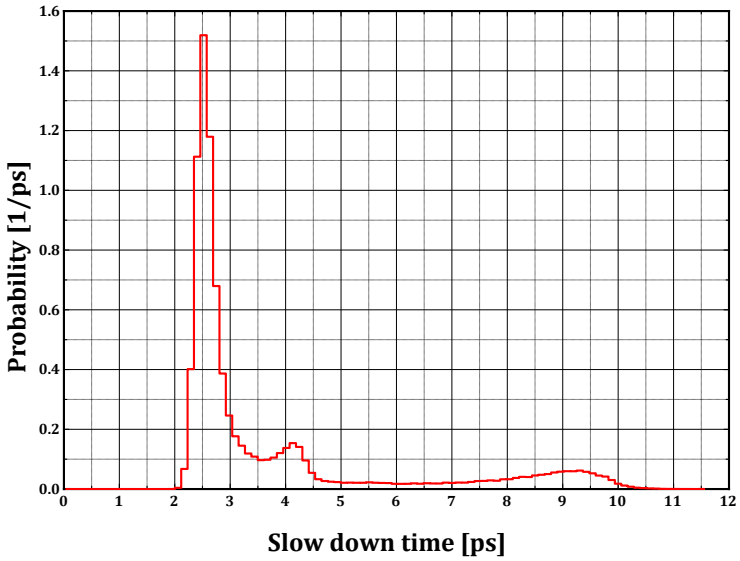

Figure 16 2 MeV He slow down time distribution

Figure 17 shows the simulated IBIC currents for the two configurations. Later we will discuss the validity of the simulation; at this point we just try to understand what we see.

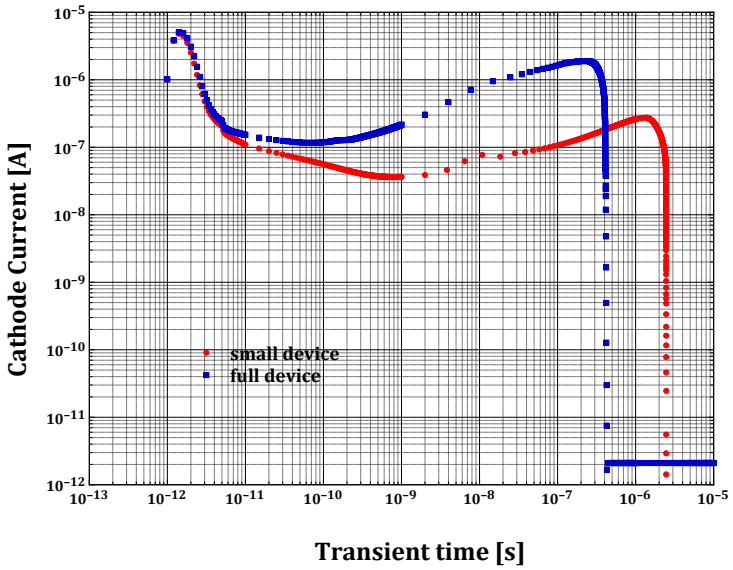

Figure 17 IBIC currents from three different configurations

In both cases there is a sharp pulse at very short times (the He ion hit the device at t = 1 ps), and then there is a long sustained current for relatively long times. For the small device it is a bit over 2 μs, for the full device it is about 300 ns, while for the full device with high doping the current lasts for hundreds of ns. This clearly illustrates the effect of size. We will only concentrate on the real device in the rest of the discussion.

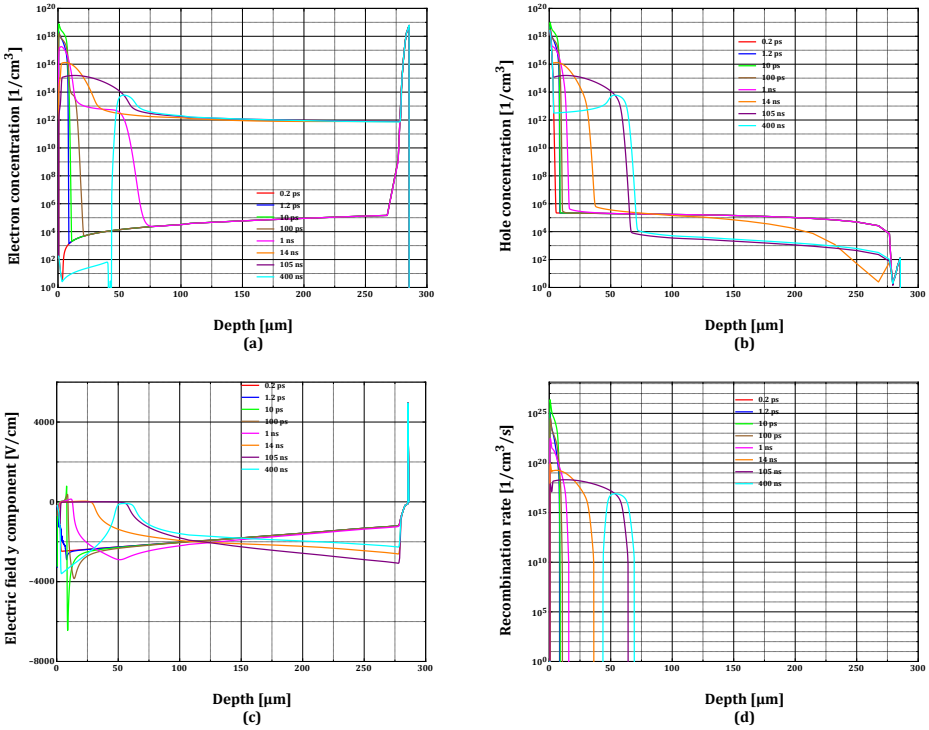

Figure 18 Carrier concentration, electric field, and recombination rate at selected times during the transient

Figure 18 shows the carrier densities, electric field, and recombination as the unction of the distance from the anode along the center of the ion track at various times during the transient. The first two curves (red and blue) are before the ion strike and right after it. By examining these curves (and the 2D distributions that will be presented at the RCM) we can interpret what is happening. The entire intrinsic layer is depleted; therefore, the charge density is the doping level, $3x10^{11}$ $1/cm^3$. When the ion hits in a very short time high-density e-h plasma is created from the surface to about 6 μm deep in the device. The electron and hole densities are several orders of magnitude larger than the doping density. At the edges of this plasma the e-h pairs are quickly separated (it initially happens in the plasma, too, but it does not create net charge) and large net charge will be present at the edges. Due to this much higher charge density than the ionized donor density, this will determine the

electrostatic properties of the devices. The electric field will be concentrated at the edges and it will be zero inside of the e-h plasma. Since the electric field is drastically changed, the Gunn theorem [23] cannot be used to describe the IBIC process. Since there is no field inside the plasma column to separate the electrons and holes, they are diffusing together toward the cathode and laterally. This movement of electrons and holes together is clearly visible in Figure 18 (a) and (b). Since this plasma density is still many orders of magnitude larger than the doping concentration, the plasma pushes the electric field ahead of itself (like a snow plow) toward the cathode as can be seen in Figure 18 c. The e-h separation occurs only at the edges. When the electron density drops below the doping concentration at the anode, the field is reastablished on the anode side of the plasma. After that the plasma is becoming smaller and less dense and eventually collapses and the electric field is restored. Figure 18 (d) shows the recombination rate. Initially the recombination rate is negative (generation) which is the source of the leakage current. During the transient the recombination rate becomes positive inside the plasma column, and the figures show very clearly that the high carrier densities and the high recombination coincide.

We can definitely see the size effect, which is due to the lateral diffusion of the carriers. As the size of the device increases, the carrier can diffuse further and the plasma will be less dense. We have to be cautious with the interpretation. This is definitely a 3D effect and it is not clear how this 2D result translates to 3D. Since we did the calculations in a 2D model, which assumes a 1 μm 3rd dimension of the device, does it mean that our ionization profile is 1 μm thick in the 3rd dimension? Another issue is that the e-h pairs are not really created by the ions but by delta electrons. If they are carrying the energy much farther than the ~ 100 nm track size, that can lower the e-h plasma density and decrease the effect. So would do a 3D model.

Conclusions

We analyzed 8 MeV He and neutron irradiated devices when the entire area was irradiated using C-V, DLTS, and IBIC. We found that the most serious problem in these devices is the increase of the leakage current, especially in the Helsinki diodes due to their large size. Unfortunately, both C-V and DLTS measurements require the irradiation of the entire device. At this point our recommendation is to do two sets of experiments, one irradiating the entire device for C-V and DLTS, and the second one creating damage locally by a nuclear microbeam. The second set of irradiation can be followed by the IBIC analysis.

We investigated several commercial devices that might be a better choice for these studies. These were Hamamatsu PIN and PN diodes. The devices were irradiated with neutrons and then C-V and IBIC measurements were performed. We found that the PINs had the same problems despite the fact that their intrinsic layer has a doping level two orders of magnitude higher than the Helsinki diodes. Even relatively small damage can create defect density in the order of the doping level. The charge that trapped in the defects can change the electrostatic configuration of the device.

This poses a serious problem for modeling, which assumes that the electric field does not change.
A 2D TCAD model of the n-type Helsinki diode was built using Silvaco's ATLAS software. A good agreement was achieved with the experimental data (C-V and I-V). The IBIC simulation of the undamaged diode showed that the e-h hole plasma created by a 2 MeV He ion pushes out the electric field and slowly diffuses until its density falls below the doping density. This leads to a very long IBIC signal and increases recombination. One has to be very careful about the interpretation of these results. This is a 2D model and it is clear that the dimensionality and the size of the model have serious effects. We recommend continuing these studies and attempting to build a 3D model, which will describe the problem better. In addition, TRIBIC experiments should be performed trying to verify the existence of this problem.

Unfortunately, due to budget cuts the support for this work completely disappeared at SNL.

References

[1] Z. Pastuovic, Progress report of ANSTO for IAEA CRP F11016, International Atomic Energy Agency, 2014.
[2] S. Rath, Progress report of University of New Delhi for IAEA CRP F11016, International Atomic Energy Agency, 2014.
[3] G. Vizkelethy, Annual report of Sandia National Laboratories (SNL) contribu-tion to IAEA CRP F11016 on "Utilization of ion accelerators for studying and modeling of radiation induced defects in semicon-ductors and insulators", International Atomic Energy Agency, 2013.
[4] R.M. Fleming, C.H. Seager, D.V. Lang, E. Bielejec, J.M. Campbell, Defect-driven gain bistability in neutron damaged, silicon bipolar transistors, Applied Physics Letters, 90 (2007) 172105.
[5] E. Bielejec, G. Vizkelethy, R.M. Fleming, D.B. King, Metrics for Comparison Between Displacement Damage due to Ion Beam and Neutron Irradiation in Silicon BJTs, IEEE Transactions on Nuclear Science, 54 (2007) 2282-2287.
[6] E. Bielejec, G. Vizkelethy, R.M. Fleming, W.R. Wampler, S.A. Myers, D.B. King, Comparison Between Experimental and Simulation Results for Ion Beam and Neutron Irradiations in Silicon Bipolar Junction Transistors, IEEE Transactions on Nuclear Science, 55 (2008) 3055-3059.
[7] E. Bielejec, G. Vizkelethy, N.R. Kolb, D.B. King, B.L. Doyle, Damage equivalence of heavy ions in silicon bipolar junction transistors, IEEE Transactions on Nuclear Science, 53 (2006) 3681-3686.
[8] E. Tuovinen, Processing of radiation hard particle detectors on Czochralski silicon, Department of Micro and Nanosciences, University of Helsinki, Espoo, Finland, 2008.
[9] M.T. Robinson, I.M. Torrens, Computer simulation of atomic-displacement cascades in solids in the binary-collision approximation, Physical Review B, 9 (1974) 5008.
[10] M. Hou, Linear collision sequences in fcc and Ll(2) metals: A computer simulation study, Nuclear Instruments & Methods in Physics Research Section B-Beam Interactions with Materials and Atoms, 187 (2002) 20-35.
[11] R.C. Fletcher, W.L. Brown, Annealing of bombardment damage in a diamond-type lattice - Theoretical, Physical Review, 92 (1953) 585-590.
[12] M. Hou, C.J. Ortiz, C.S. Becquart, C. Domain, U. Sarkar, A. Debacker, Microstructure evolution of irradiated tungsten: Crystal effects in He and H implantation as modelled in the Binary Collision Approximation, Journal of Nuclear Materials, 403 (2010) 89-100.
[13] M. Jaraiz, J. Arias, L.A. Bailon, J.J. Barbolla, Detailed computer-simulation of damage accumulation in ion irradiated crystalline targets, Vacuum, 44 (1993) 321-323.
[14] K.M. Klein, C.H. Park, A.F. Tasch, Modeling of commulative damage effects on ion-implantation profiles, Nuclear Instruments & Methods in Physics Research Section B-Beam Interactions with Materials and Atoms, 59 (1991) 60-64.

[15] A. Scholz, C. Lehmann, Stability Problems, Low-Energy-Recoil Events, and Vibrational Behavior of Point Defects in Metals, Physical Review B, 6 (1972) 813-826.
[16] A. Souidi, M. Hou, C.S. Becquart, C. Domain, Atomic displacement cascade distributions in iron, Journal of Nuclear Materials, 295 (2001) 179-188.
[17] M.T. Robinson, MARLOWE: Computer Simulation of Atomic Collisions in Crystalline Solids (Version 15b), Radiation Safety Information Computational Center (RSICC), Oak Ridge National Laboratory, Oak Ridge, TN, 2002.
[18] M.T. Robinson, Binding energy effects in cascade evolution and sputtering, Nuclear Instruments & Methods in Physics Research Section B-Beam Interactions with Materials and Atoms, 115 (1996) 549-553.
[19] G. Vizkelethy, S.M. Foiles, To be published.
[20] ATLAS User's Manual, Silvaco, Inc., 2013.
[21] E. Vittone, Electrostatic model of the n-type diode N. 26 from Helsinki Institute of physics, International Atomic Energy Agency, 2012.
[22] J.F. Ziegler, SRIM, http://www.srim.org, 2008.
[23] J.B. Gunn, A General Expression for Electrostatic Induction and its Application to Semiconductor Devices, Solid-State Electronics, 7 (1964) 739-742.